Revision 2

A micro-reflectance IR spectroscopy method for analyzing volatile species in basaltic, andesitic, phonolitic and rhyolitic glasses

Penelope L. King[1, 2, 3] and Jessica F. Larsen[4]

1. Research School of Earth Sciences, Australian National University, Canberra ACT 0200 Australia.

2. Institute for Meteoritics, University of New Mexico, Albuquerque NM 87131 USA.

2. Dept. Earth Sciences, University Western Ontario, London ON N6A 5B7 Canada.

3. Geophysical Institute, University of Alaska, Fairbanks, AK 99775 USA.

* Present address.

ABSTRACT

Volatile contents of geologic glasses are used to model magma chamber and degassing processes, thus, there is considerable interest in small-scale analytical techniques for analyzing volatiles in glasses. Infrared (IR) spectroscopy has the advantage of determining volatile speciation in glasses (e.g., OH^-, molecular H_2O, molecular CO_2 and CO_3^{2-}). However, sample preparation for the most common IR method used, micro-transmission IR spectroscopy, is complicated because glasses must be prepared as thin parallel sided-wafers. Raman analysis, while valuable for Fe-poor samples, can be difficult to use for Fe-rich glasses.

We have calibrated a micro-reflectance infrared method for determining volatile species using calculated Kramers-Kronig absorbance (KK-Abs.) spectra that requires that only one side of a glass be polished. The method is easier to use than other reflectance methods where it is difficult to determine the baseline for the IR bands. Total H_2O wt.% = m * (3600 cm^{-1} KK-Abs.), where m, is the slope of the calibration line that is obtained from a fit to the data. The m value is

related to the calculated refractive index, *n*, for a range of aluminosilicate glass compositions allowing the technique to be applied to samples with unknown calibration slopes. For calc-alkaline andesite glasses we determined calibration slopes for micro-reflectance IR measurements of molecular H_2O, molecular CO_2, and CO_3^{2-}. The method has been calibrated for glasses with up to 6.76 wt.% total H_2O (but is useful for glasses with more than 20 wt.% total H_2O) and has been calibrated for glasses with up to 0.575 wt.% total CO_2.

This technique provides a means to analyze volatile abundances in samples that are not possible to analyze or prepare for analysis with transmission micro-IR techniques. We have determined volatile contents in fragile samples such as cracked, vesicular or crystal-bearing glasses formed by volcanic or impact processes or in high pressure bubble nucleation experiments and H diffusion experiments. We have monitored H uptake during weathering of basaltic glasses that cannot be polished and determined volatiles in melt inclusions and pumice.

Key words: IR spectroscopy, glass properties, new technique, volatiles, H_2O, CO_2, CO_3^{2-}

INTRODUCTION

Volatiles, such as H_2O and CO_2, are found in natural glasses and their abundances are used to model the role of volatiles on magmatic processes and degassing (Wallace and Anderson Jr., 2000; Larsen and Gardner, 2004; Métrich and Wallace, 2008); to determine volatile diffusion rates in melts (e.g., Liu et al., 2004); and to measure volatile contents of impact glasses (Harris et al., 2007). Thus, there is considerable interest in small-scale analytical techniques for analyzing glasses. A variety of techniques are used, such as vacuum-line manometry, secondary ion mass spectrometry, Karl-Fischer titration (for H_2O), Raman spectroscopy, and Fourier transform infrared (FTIR) spectroscopy (see reviews in Ihinger et al., 1994; Deloule et al., 1995; Devine et

al., 1995; King et al., 2002; Behrens et al., 2006; Thomas et al., 2006; Aubaud et al., 2007). Of these techniques, only Raman and FTIR spectroscopy provide information on volatile species (e.g., OH^-, molecular H_2O (H_2O_{mol}), molecular CO_2 ($CO_{2\ mol}$) and CO_3^{2-}) in small sample areas (< 50 μm across). The abundances of these species are also used in volcanic 'geospeedometers' (e.g., Zhang et al., 2000) and it is therefore advantageous to measure them accurately.

Micro-Raman spectroscopy has been developed to determine the total H_2O (H_2O_{tot}), H_2O_{mol} and OH^- in silicic, Fe-poor glasses (Thomas, 2000; Chabiron et al., 2004; Behrens et al., 2006; Thomas et al., 2006) and a few Fe-bearing glasses (Chabiron et al., 2004; Zajacz et al., 2005; Behrens et al., 2006; di Muro et al., 2006; Thomas et al., 2008a; Mercier et al., 2009). Raman methods use either internal calibrations (e.g., Behrens et al., 2006) or a comparator method where samples are referenced to one calibration glass (Thomas et al., 2008b). However, there are difficulties in applying the micro-Raman method to Fe-bearing glasses due to band overlap in the 100–1100 cm^{-1} region and absorption of the laser radiation with depth in Fe-bearing glasses that decreases the OH band intensity (Behrens et al., 2006; Thomas et al., 2008a). In addition, glasses with low melting temperatures, including water-rich samples, may lose volatiles or melt due to strong light absorption and/or fluorescence radiation.

FTIR spectroscopy has been used to successfully analyze Fe-rich compositions like basaltic glasses (e.g., Dixon et al., 1988; Dixon and Pan, 1995). However, the most common method used, micro-transmission IR spectroscopy, is complicated because glasses are generally prepared as thin, parallel-sided, stand-alone wafers (e.g., Paterson, 1982; Stolper, 1982a, b; Newman et al., 1986; Dixon et al., 1988; Ihinger et al., 1994; Dixon and Pan, 1995). Transmission IR techniques using ground glass powders pressed into a KBr disc have the advantage that painstaking thickness measurements on doubly polished glass wafers are not

required; however KBr is hygroscopic and therefore it is challenging to ensure that water is not adsorbed (e.g., Izawa et al., 2010). Furthermore, the KBr method is not appropriate for samples in which spatially constrained, fine-scale spectra are needed such as melt inclusions and some experimental glasses. A technique has been developed to investigate melt inclusions in doubly polished olivine crystals (Nichols and Wysoczanski, 2007); however that technique is not amenable to studying very small melt inclusions and some volatile species are not possible to measure (e.g., H_2O_{mol}) due to band interferences from the host mineral. An alternative technique is micro-reflectance IR analysis (e.g., Grzechnik et al., 1996; Moore et al., 2000; Hervig et al., 2003), where only one sample face is polished.

The major advantage of the micro-reflectance method is that the sample can be prepared as a single polished surface. Therefore, small samples, such as melt inclusions, do not need to be removed from their matrix for mounting and fragile pumices and experimental charges may be analyzed in textural context. Also, different depths within a single sample can be analyzed sequentially by successively polishing the sample to deeper levels.

Previous work has shown that reflectance spectra for C-O-H volatiles have band positions similar to that found in transmission IR spectra, but they have different shapes due to the mathematical nature of the superposition of the volatile bands on the Si-O band. Example micro-reflectance IR spectra are shown in Figure 1a and 1b.

For O-H species in glasses, the largest band occurs as a "negative band" in the 3500 cm^{-1} region (Hervig et al., 2003). This band, referred to here as a “total H_2O” band, arises from a combination of symmetric stretching of the H-O-H molecule (ν_{ss}H-O-H), plus symmetric stretching of Si-OH (ν_{ss}Si-OH) in the aluminosilicate network, plus an overtone of the H-O-H bending vibrations (2δH-O-H). The asymmetric stretching vibration (ν_{as}) of $CO_{2\ mol}$ gives rise to

a "sigmoidal" feature in the reflectivity spectrum (Moore et al., 2000). The dissolved CO_3^{2-} concentrations (νC-O) in basanite and leucitite glasses have a "doublet" band in micro-reflectance IR spectra that resembles the absorption bands obtained in transmission IR studies (Grzechnik et al., 1996). In this study, we show that a "negative band" for molecular H_2O related to H-O-H bending vibrations (δHOH) occurs in the ~1620 cm^{-1} region, in agreement with the band observed in transmission IR spectra.

In micro-reflectance IR measurements, H_2O_{tot} and total CO_2 ($CO_{2\ tot}$) concentrations have been related directly to the height of the reflectance band for the species of interest (ΔR_i) relative to the reflectance at a reference wavenumber position (R_{ref}) via an empirical equation of the form:

$$(\Delta R_i/R_{ref}) = k_1 * (\text{volatile species \%}) + k_2 \quad (1)$$

where the positions of the ΔR_i and R_{ref} and the constants k_1 and k_2 depend on the glass composition (see King et al., 2004).

Despite, the ease of micro-reflectance IR measurements, the extraction of band heights from raw R% spectra may be somewhat challenging (e.g., Fig. 1a, 1b). There are significant uncertainties associated with the baseline position, especially for samples with low volatile contents and for sigmoidal bands like $CO_{2\ mol}$ and H_2O_{mol} (Fig. 1a, 1b). Also, assumptions are needed regarding the location of R_{ref} for different composition glasses. Furthermore, calibrations are not available for H_2O_{tot} or H_2O_{mol} in basalt, or C-O species or H_2O_{mol} in andesite.

In this paper, we present a method for analyzing glasses using micro-reflectance IR spectroscopy that has been manipulated using a Kramers-Kronig (KK) transform. The technique is advantageous because it is straightforward to prepare samples and easier to determine the baseline position for IR bands than using the raw R% spectra. We provide new calibration curves

for basalt, calc-alkaline andesite, alkali andesite, phonolite and rhyolite. We also examine some of the limitations of this technique.

METHODS

Volatile-bearing glasses were obtained (Perfit et al., 1983, 1999; Westrich, 1987; Moore and Carmichael, 1998; King et al., 2002; Sinton et al., 2003; Larsen and Gardner, 2004; Lui, 2005; Mongrain et al., 2008) and their compositions were confirmed using the electron microprobe if necessary (Table 1). The basaltic glasses were analyzed using transmission IR spectroscopy and the H_2O_{tot} concentrations determined with the Beer-Lambert law (e.g., Stolper, 1982b):

$$\text{molar concentration of } H_2O_{tot} = A / (d * \rho * \varepsilon_{H_2O_{tot}}) \quad (2)$$

where, A is the linear absorbance (i.e. band height), d is the sample thickness which was measured with a Mituyomo micrometer to ± 2 μm (<2% relative error for most samples); ρ is the sample density that was calculated following methods in Silver (1988) and data from Church and Johnson (1980) and Mandarino (1976); and $\varepsilon_{H_2O_{tot}}$ is the extinction coefficient for H_2O_{tot} in basalt (from Dixon et al., 1995). Calc-alkaline andesite glasses contained both C-O species as well as H-O species. Table 1 shows that variations in volatile-free composition were negligible for most glasses. In the case of the basalt and rhyolite 1σ deviations are given because slightly different compositions constitute the sample set. Errors in the volatile contents were taken from the literature or for the basalts and phonolite conservatively estimated using curve fitting uncertainties (10 to 14 % relative) (Table 1).

Micro-reflectance IR analyses of the glasses were collected using a Nicolet Nexus 670 spectrometer with a Globar source, extended range KBr beamsplitter (XT-KBr), and a

Continuμm microscope with a MCT-A detector (cooled with liquid nitrogen). The same instrument was used in King's lab at both the Experimental Analysis Laboratory at the University of Western Ontario and the New Mexico IR Analysis Laboratory at the University of New Mexico. Analyses were made in triplicate if possible, but some glass samples were too small for multiple analyses.

As with any IR analysis of C-O-H species, it is necessary to minimize the background levels of atmospheric gases surrounding the sample. All analyses in this work were performed by running a dry air purge into a volume around the sample that was ~ 100 cm^3 (e.g., Fig. 47 in King et al. 2004). We also monitored the total reflectance signal by examining the interferogram peak-to-peak measurement before each analysis. We prefer to operate at conditions where the peak-to-peak measurement is greater than 6.0 volts and we did not operate at conditions less than 4.0 volts.

Each spectrum was collected in a spectral range of 5300 – 650 cm^{-1}, over 300 scans, with 4 cm^{-1} resolution, using a 100 x 100 μm sampling area. For each analysis, a background spectrum was collected on a gold-coated glass slide because it has a reflection coefficient of ~100% over the wavelength region measured, and so the absolute value of the sample reflectivity is known without further calibration. The raw spectra were collected in units of percent reflectance (%R). For our purposes, 300 scans appeared to provide sufficiently high signal-to-noise ratio (SNR); however, if a small aperture IR beam is used (e.g., for small melt inclusions), it is necessary to maximize the SNR by increasing the scan times to larger values (>1000 scans, Grzechnik et al. 1996).

To convert the R% spectra to absorbance spectra we used the KK transform (McMillan and Hofmeister, 1988), recently discussed in detail by Dufresne et al. (2009). The formula for the KK transform is:

$$\theta(\nu_i) = \frac{2\nu_i}{\pi}\int_0^{\infty} \frac{\ln r(\nu) - \ln r(\nu_i)}{\nu_i^2 - \nu^2} d\nu \quad (3)$$

where θ is the phase shift, ν is the real portion of the frequency, ν_i is imaginary portion of the frequency and r is the real part of the reflectivity. In this study the reflectance spectra were transformed into KK absorbance (KK-Abs.) units by first smoothing the data points as a function of wavenumber over a ~40.5 cm^{-1} window (like Moore et al., 2000) using a "running average type" algorithm (Savitsky-Golay). A smoothed spectrum minimizes error because the subsequent KK transform requires extrapolating the wings of the reflectance spectrum (Efimov 1995). The KK transform was performed using the OMNIC software (version 6.1) and to further ensure uniform extrapolation, we sampled over a constant range of 5300 – 650 cm^{-1}.

RESULTS

Figures 1c and 1d show representative KK-Abs. spectra and illustrate the shapes of the major bands that are observed in this type of spectra (discussed above). Each spectrum was examined in the 700-1300 cm^{-1} region to verify that only a broad glass band was present, ruling out a significant volume of crystals (with sharp bands at specific wavenumbers) or issues related to internal scattering of light. The volatile bands were then studied in detail. In contrast to the subtle features observed in R% spectra (Fig. 1a, 1b), the KK-Abs. volatile species bands (Fig. 1c, 1d) form positive peaks and the CO_3^{2-} species forms a doublet, like transmission IR spectra. Each band increases in KK-Abs. intensity with increasing volatile contents (Tables 2 and 3).

The baseline under the $CO_{2\ mol}$ band is relatively linear, whereas the baselines under the CO_3^{2-} doublet and H_2O_{mol} bands are curved due to superposition on the large Si-O band. We fit the latter baselines using French curves following the techniques discussed in King et al. (2004). That work evaluated the error associated with different baseline correction approaches (e.g., fitting with Gaussian curves) and found that the French curve method allows for a conservative estimate of the fitting error (<10 % relative). We assessed reproducibility by fitting maximum and minimum baselines to the spectra and the variations were all within this conservative error (<10 % relative). The baseline under the 3600 cm^{-1} peak was assumed to be linear between 3800 and ~2800 cm^{-1}, and we assume that the line has a 10% error (e.g., King et al., 2002).

Total H_2O contents

The KK-Abs. for the H_2O_{tot} band measured from a linear baseline has good reproducibility, with: 1σ < 5% for 3-4 replicates on most samples and always < 20% (e.g., Tables 2 and 3). For each composition, the H_2O_{tot} KK-Abs. increases linearly as a function of H_2O_{tot} wt.% (Fig. 2), following the relation:

$$H_2O_{tot}\ \text{wt.\%} = m * (3550\ cm^{-1}\ \text{band KK-Abs.}) \quad (4)$$

where m, the slope of the calibration line, is a function of composition. The following are compositions/m/r^2 of the fit: calc-alkaline andesite/154/0.93; alkali andesite/156/0.99; phonolite/172/0.90; and rhyolite/204/0.99. Our calibration slope for phonolite was presented in Mongrain et al. (2008) and our approach was used by Pauly et al. (2011), but the calibration data were not shown in either case. We chose to force equation 4 through zero because there should be no IR signal when H_2O_{tot} is absent.

The calibration slope for the basaltic glasses (m = 125, r^2 = 0.97) is essentially defined by the sample with the high water content and so we suggest that this is a preliminary value. Also,

the basaltic glasses with low water contents are all natural samples and may show more scatter because they have greater variation in composition and may have more intrinsic variation in water contents. Nonetheless, we are encouraged that Pauly et al. (2011) found a similar slope for palagonite (m = 123) when comparing KK-Abs. values to electron microprobe deficits.

Molecular H_2O, molecular CO_2 and carbonate contents

The H_2O_{mol} and $CO_{2\ mol}$ bands are relatively easy to identify in both the reflectance and KK-Abs. spectra because both form strong, narrow peaks (low degeneracy in the molecular vibration). In contrast, the CO_3^{2-} doublet at these concentrations is not possible to identify in reflectance spectra (Fig. 1a; cf. Grzechnik et al., 1996; Moore et al., 2000) although the KK-Abs. spectra have a discernable CO_3^{2-} doublet (Fig. 1c).

For the calc-alkaline andesite glasses we found the following relations: H_2O_{mol} = 435*(1620 cm^{-1} KK-Abs.), r^2 = 0.92, $CO_{2\ mol}$ = 37.2 * (2350 cm^{-1} KK-Abs.), r^2 = 0.91; and CO_3^{2-} = 500 * (1520 cm^{-1} KK-Abs.), r^2 = 0.74. The data used to constrain these equations are shown in Figures 3-5 and, again, we chose to force the fit through zero. The most difficult volatile to quantify with our technique is CO_3^{2-} based on the large scatter about the calibration line (Fig. 5), likely due to the nature of the CO_3^{2-} vibration and its resulting IR doublet band.

In sum, these results indicate that H_2O_{tot}, H_2O_{mol}, $CO_{2\ mol}$ and possibly CO_3^{2-} may be quantified in aluminosilicate glasses using reflectance IR techniques. We anticipate that the technique may be further developed to quantify C-O-H species in a range of aluminosilicate compositions.

DISCUSSION

Errors in regression analysis

To examine the goodness of fit (precision) of the calibration line with an ordinary least squares fit, we determined how the calibration line fit varied when using a robust regression, employing the Isoplot program for Excel (Ludwig, 2003). The purpose of using the robust regression is to examine whether outliers in the data might artificially influence the line fits and to also estimate how the slope of the calibration lines may vary accounting for the scatter in the data used for each composition. When forced through zero, the robust regression returns slopes that are within 7 % of those determined using the ordinary least squares fit (Table 4). The errors on the slope of the line determined using the robust regression method vary from 5 to 10 % (Table 4). This is comparable with other methods, such as SIMS, where the data used for calibrations has +/- 10% relative error. In contrast, errors on transmission FTIR and manometry data can be significantly smaller in the case of high quality data where exceptional care is taken with the analyses. However, the error on transmission FTIR analyses is commonly significant in the case where thickness estimates are difficult, and thus the error on the analysis commonly approaches 10% or more (King et al., 2004).

In order to examine the predictive nature (accuracy) of the linear regressions for determining the compositions of unknown samples, we report the root mean square error prediction (RMSEP). This value provides a way to estimate the accuracy error involved in using the calibration line to predict the volatile content of an unknown sample. RMSEP values take into account the measurement errors, random errors, prediction errors (residuals) and bias. Values of RMSEP that are close to zero indicate smaller prediction errors for the linear regression. The formula for RMSEP is:

$$\text{RMSEP} = \sqrt{\frac{1}{n}\sum_{i=1}^{n}(y_i - \hat{y}_i)^2} \quad (5)$$

where, *n* is the number of measurements in the calibration set (including a sample with 0% of the volatile), *i* refers to a particular observation, and $\hat{y}_i$ is the predicted value derived from a linear regression on the calibration set leaving out the measured value for that observation (i.e. a jack-knife or segmented approach). For H_2O_{tot}, the RMSEP values given in Table 4 have a range of 0.10 wt.% (rhyolite) to 0.20 wt.% (alkali andesite) for the linear fits. For the calc-alkaline glasses, very good prediction errors are observed for H_2O_{mol} (RMSEP = 0.16 wt.%; Fig. 3) and for $CO_{2\ mol}$ (RMSEP = 0.003 wt.%; Fig. 4) for linear fits. The CO_3^{2-} contents were so poorly correlated with the 1520 cm^{-1} band height that we did consider it useful to calculate the RMSEP. The RMSEP are larger for the robust linear regressions (Table 4), as would be expected since those fits include errors due to outliers. The andesites, rhyolite and basalt glasses show a small differences (up to 4 wt.%) between the RMSEP for the standard linear regression versus the robust linear regression, which indicates that the accuracy is for these glasses not greatly affected by outliers. The difference is greater for the phonolites (standard RMSEP = 0.19 wt.% versus robust RMSEP = 0.38 wt.%), indicating that outliers do affect the phonolite calibration curves. In general, the RMSEP indicate that this method has accuracy errors for samples with 1 wt.% H_2O_{total} that are less than 20% relative, with the relative accuracy improving at higher H_2O_{tot} contents.

A general model for micro-reflectance IR measurements of total H_2O

A systematic increase in the calibration slope for H_2O_{tot}, *m*, with increasingly more mafic compositions is observed in the linear least squares fit calibration lines (Fig. 2 and Table 4), as well as in the robust regressions (Table 4). Such a systematic change suggests that there is a compositional or optical control on the calibration slope, similar to that observed for extinction

coefficients determined by transmission IR spectroscopy (e.g., Dixon et al., 1995; Jakobsson, 1997; Mandeville et al., 2002). We observe a reasonable negative correlation between (Si + Al) mole fraction and the calibration slope, *m* (Table 4). However, a better correlation is observed between the calculated refractive index, *n*, and *m* (Table 4 and Fig. 6) for both types of fits. We hypothesize that this correlation indicates that the optical properties of the glass are the major control on the slopes of the calibration lines. This finding indicates significant promise in developing a general reflectance IR calibration that covers a range of aluminosilicate glass compositions.

Analysis of glass wafers

Figure 7a shows the type of spectrum observed when a calc-alkaline glass wafer (in this case 90 μm) is placed on a Au-coated glass slide and analyzed in reflection mode (referred to hereafter as "wafer reflectance"). Instead of a reflectance spectrum (Fig. 1a), the wafer reflectance spectrum (Fig. 7a) has strong similarities to a transmission spectrum (Fig. 7b) combined with a KK-Abs. spectrum (Fig. 1b). This effect is likely due to some of the light transmitting through the sample, being reflected by the Au-coated glass slide substrate, and returning to the detector in addition to some signal reflecting off the surface of the glass. Mixed transmission-reflectance behavior is supported by the observation that both the transmission and reflectance features are affected by thickness of the sample (Fig. 8). For example, in calc-alkaline andesite samples that are <~100 μm both transmission and reflectance features are observed whereas those that are thicker show reflectance features only (like Fig. 1a). However, the thickness at which the behavior of the IR light through a wafer changes from mixed to reflectance is expected to depend on refractive index (a function of composition). Previous studies that only observed transmission features for rhyolites on a Au backing (Nowak and

Behrens, 1995) only examined the near-IR part of the spectrum where transmission features dominate and therefore the reflectance features were not observed.

In the wafer reflectance spectrum, the KK-Abs.intensity is amplified: relative to the transmission spectrum, the amount of absorbance amplification is a function of the wavenumber. For example, absorbance for H_2O_{tot} and $CO_{2\ mol}$ are amplified ~2x, whereas absorbance for CO_3^{2-} is amplified ~1.5x (Figs. 7a, 7b). We predict that the absorbance amplification is non-linear due to variations in the optical constants of the glass at different frequencies (e.g. refractive index, dielectric constant etc.). Therefore, glasses of different compositions likely have specific "wafer reflectance calibration coefficients", $m_{WR,\ species}$, for each of the volatile species similar to transmission IR spectroscopy. Until we have better constrained $m_{WR,\ species}$, it would be advantageous to minimize the effect of transmission in a thin sample. For example, melt inclusions are commonly <100 μm and thin sections are ~30 μm; thus both types of samples provide the impetus for developing this micro-reflectance IR technique for thinner glass wafers.

To this end, we experimented with roughening the back of andesite wafers that were less than 100 μm thick. Figure 8a shows reflectance spectra for a calc-alkaline andesite glass wafer (MHA31, initially a 60 μm thick wafer) roughened on the back to 1 μm, 40 μm and 90 μm. The spectra are seen to become progressively less transmission-like and more reflectance-like with increasing roughness. Unfortunately, the wafer was damaged when it was roughened with 200 μm grit. However, Figure 8b shows a different andesitic glass wafer (MHA-44, initially a 63 μm thick wafer) roughened with a ~130 μm polishing grit and set in epoxy resulted in an almost ‘pure’ reflectance spectrum. The reflectance spectrum from the roughened sample was converted to KK-Abs. units, resulting in a spectrum that is very similar to a KK-Abs. spectrum derived from a reflectance spectrum collected from a thick glass (Fig. 9). The total water content

315 calculated using these two KK-Abs. spectra was identical, with both spectra giving 4 wt.%
316 H_2O_{tot}. This value is within error of the measured H_2O_{tot} content of 3.34 wt.%.

317 In sum, glass wafers may be analyzed with reflectance techniques using samples where
318 the back has been roughened to ~130 μm and set in epoxy. However, glass wafer methods
319 deserve further development because spectra collected on such samples have the advantage of
320 higher absorbance signal (Fig. 7a) and would be useful for analysis of melt inclusion and thin
321 sections.

322 **Interlaboratory comparison, comparison of IR detectors and caveats**

323 To determine if our reflectance IR technique depends on the instrument set-up we
324 undertook two separate studies. First, measurements were made using different detector types
325 (MCT-A* versus MCT-A in King's lab); and second, we measured the phonolite glasses at the
326 University of Alaska (Larsen's lab). The MCT-A detector has a lower detectability rating (D* =
327 4.5×10^{10}) than the MCT-A* (D* = 6.5×10^{10}) according to the manufacturer (ThermoFisher).
328 Larsen's lab uses a Nicolet 6700 FTIR (compared to King's Nicolet Nexus 670), but both used a
329 Globar source, XT-KBr beamsplitter, and a Continuμm microscope with a liquid nitrogen cooled
330 MCT-A detector.

331 Figure 10a shows that the KK-Abs. value for H_2O_{tot} using the MCT-A* detector is
332 consistently lower than that determined using the MCT-A detector (Fig.10a). This result is
333 surprising because the MCT-A* detector is designed with higher detectability, thus we cannot
334 rule out detector alignment issues. Nonetheless, the data show that such variables (detector,
335 alignment etc.) are important for accurate calibration curves.

336 Figure 10b shows the results of phonolite analyses in Larsen's lab using the spectrometer
337 configuration noted above. The reflectance peak heights from Larsen's lab are systematically

higher than those obtained in King's lab using an older instrument, although some results are within error (Fig. 10b).

Together, the results of analyses with different machine configurations indicate that volatile calibration curves depend on a particular instrument's configuration (e.g., light throughput and detector efficiency). Therefore, to use these techniques it is necessary to create instrument-specific calibration curves and to check these periodically. This is similar to other micro-analytical techniques currently used for volatiles that also depend on instrument set-up and efficiency, such as secondary ion mass spectrometry (SIMS) and Raman spectroscopy. One of the advantages of the IR method relative to SIMS is that "blanks" as well as calibration standards do not need to be measured at each analytical session. Furthermore, we have shown that the IR calibrations for H_2O_{tot} are related to calculated refractive indices, which means that once calibrations have been done in a laboratory using certain glass compositions that it is possible to estimate the slope of the calibration line, m, to determine H_2O_{tot} in other compositions.

As implied above, the KK transform results are sensitive to the input parameters, especially the wavelength range. Smoothing to window spacings that are slightly different results in negligible changes to the calculated KK-Abs. spectrum. However, we find that spectra that are measured over different wavelength ranges do not necessarily give the same KK-Abs. as our technique measured over 5300 – 650 cm^{-1} due to variations in extrapolating the wings of the reflectance spectrum prior to KK transformation. Despite the potential *accuracy* errors associated with the wavelength extrapolation, this study shows that two laboratories or different detectors produce results with similar *precision* errors. Furthermore, the technique produces slopes for the calibration lines for a range of glass compositions that may be logically explained through a

360 physical property of the glass: the refractive index. We recommend using the same spectral range
361 as our measurements when using our approach.

362 **Application of the micro-reflectance IR techniques to challenging samples**

363 We have been able to determine volatile contents in fragile experiments on bubble
364 nucleation (Mongrain et al., 2008) and H_2O_{tot} diffusion from wet basaltic to dry rhyolitic melt
365 (glass) (Lui, 2005). We have monitored H_2O_{tot} uptake during weathering of basaltic glasses that
366 cannot be polished (our unpublished data) and others have measured H_2O_{tot} contents of fragile
367 palagonites (Pauly et al., 2011). Also, we have measured the H_2O_{tot} content of fragile impact
368 melt glasses (Harris et al., 2007). The impact glasses had in excess of 20 wt.% H_2O_{tot} determined
369 by alternate methods (Harris et al., 2007) and would have been exceedingly difficult to prepare
370 as very thin wafers for micro-transmission IR analyses; thus, the reflectance method is
371 advantageous for unusually H-rich samples. We recommend that the μ-R-IR technique is best for
372 samples with high volatile contents. In such samples, the method allows for rapid determination
373 of the H_2O_{tot} and H_2O_{mol} contents.

374 Our findings are consistent with technique development using attenuated total reflection
375 (ATR; Lowenstern and Pitcher, submitted) and synchrotron reflectance IR techniques. Combined
376 with these techniques, IR analysis with a mapping stage with overlapping spectral collection
377 (several micron stepsize) should improve the areal resolution of micro-reflectance IR analyses
378 and potentially allow smaller volumes to be sampled than with transmission IR methods which
379 are commonly limited by the thickness of the sample. Spectra can be obtained on glassy areas
380 and checked for the presence of minerals by verifying that the 700-1300 cm^{-1} region only
381 contains a broad glass band.

382

ACKNOWLEDGEMENTS

We thank Sylvia-Monique Thomas and an anonymous reviewer for helpful comments that improved the manuscript. We thank Gordon Moore and Hank Westrich for loaning us their alkali andesite and rhyolite glasses, and Michael Perfit, Dan Lui and John Sinton for their basaltic glasses. We are grateful for discussions with Kim Dalby, Dan Lui, Larry Anovitz, Peter Michael, Grant Henderson and Darby Dyar on aspects of the manuscript. Theresa Serwatuk did some of the initial analyses and Jo Mongrain did some of the phonolite analyses. Paul McMillan and Jake Lowenstern introduced PLK to IR techniques for analyzing volatiles in glasses. PLK was supported by grants from Canadian NSERC, CFI and NSF-EAR 0911224 (C. Agee) and 1019558 (M. Ramsey). JFL was supported by NSF 0511070.

REFERENCES

Aubaud, C., Withers, A.C., Hirschmann, M.M., Guan, Y., Leshin, L.A., Mackwell, S.J., and Bell, D.R. (2007) Intercalibration of FTIR and SIMS for hydrogen measurements in glasses and nominally anhydrous minerals. American Mineralogist, 92, 811-828.

Behrens, H., Roux, J., Neuville, D.R., and Siemann, M. (2006) Quantification of dissolved H_2O in silicate glasses using confocal micro-Raman spectroscopy. Chemical Geology, 229, 96-112.

Chabiron, A., Pironon, J., and Massare, D. (2004) Characterization of water in synthetic rhyolitic glasses and natural melt inclusions by Raman spectroscopy. Contributions to Mineralogy and Petrology, 146, 485–492.

Church, B.N., and Johnson, W.N. (1980) Calculation of the refractive index of silicate glasses from chemical composition. Geological Society of America Bulletin, 91, 619-625.

Deloule, E., Paillat, O., Pichavant, M., and Scaillat, B. (1995) Ion microprobe determination of water in silicate glasses: methods and applications. Chemical Geology, 125, 19-28.

Devine, J.D., Gardner, J.E., Brach, H.P., Layne, G.D., and Rutherford, M.J. (1995) Comparison of microanalytical methods for estimation of H_2O contents of silicic volcanic glasses. American Mineralogist, 80, 319-328.

di Muro, A., Villemant, B., Montagnac, G., Scaillet, B., and Reynard, B. (2006) Quantification of water content and speciation in natural silicic glasses (phonolite, dacite, rhyolite) by confocal microRaman specrometry. Geochimica et Cosmochimica Acta, 70, 2868-2884.

Dixon, J.E., and Pan, V. (1995) Determination of the molar absorptivity of dissolved carbonate in basanitic glass. American Mineralogist, 80, 1339-1342.

Dixon, J.E., Stolper, E., and Delaney, J.R. (1988) Infrared spectroscopic measurements of CO_2 and H_2O in Juan de Fuca Ridge basaltic glasses. Earth and Planetary Science Letters, 90, 87-104.

Dixon, J.E., Stolper, E.M., and Holloway, J.R. (1995) An experimental study of water and carbon dioxide solubilities in mid-ocean ridge basaltic liquids. Part I: Calibration and solubility models. Journal of Petrology, 36, 1607-1631.

Dufresne, C.D.M., King, P.L., Dyar, M.D., and Dalby, K.N. (2009) Effect of SiO_2, total FeO, Fe^{3+}/Fe^{2+}, and alkali elements in basaltic glasses on mid-infrared spectra. American Mineralogist, 94, 1580-1590.

Efimov, A.M. (1995) Optical Constants of inorganic Glasses. p. 224. CRC Press, Boca Raton.

Grzechnik, A., Zimmerman, H.D., Hervig, R.L., King, P.L., and McMillan, P.F. (1996) FTIR micro-reflectance measurements of the CO_3^{2-} ion content in basanite and leucitite glasses. Contributions to Mineralogy and Petrology, 125, 311-318.

Harris, R.S., Schultz, P.H., and King, P.L. (2007) The fate of water in melts produced during natural and experimental impacts into wet, fine-grained sedimentary targets. Workshop on Impact Cratering II, Lunar Planetary Institute, Abstr. #8051.

Hervig, R.L., Mazdab, F.K., Moore, G., and McMillan, P.F. (2003) Analyzing hydrogen (H_2O) in silicate glass by secondary ion mass spectrometry and reflectance Fourier transform infrared spectroscopy. In B. de Vivo, and R.J. Bodnar, Eds. Developments in Volcanology, 5, Melt Inclusions in Volcanic Systems: Methods, Applications and Problems, p. 83-103. Elsevier, Amsterdam.

Ihinger, P.D., Hervig, R.L., and McMillan, P.F. (1994) Analytical methods for volatiles in glasses. In M.R. Carroll, and J.R. Holloway, Eds. Reviews in Mineralogy, 30, p. 67-121. Mineralogical Society of America, Washington DC.

Izawa, M.R.M., King, P.L., Flemming, R.L., Peterson, R.C. and McCausland, P.J.A. (2010) Mineralogical and spectroscopic investigation of enstatite chondrites by X-ray diffraction and infrared reflectance spectroscopy. Journal of Geophysical Research – Planets, 115, doi:10.1029/2009JE003452.

Jakobsson, S. (1997) Solubility of water and carbon dioxide in an icelandite at 1400 °C and 10 kilobars. Contributions to Mineralogy and Petrology, 127, 129-135.

King, P.L., Vennemann, T., Holloway, J., Hervig, R., Lowenstern, J., and Forneris, J. (2002) Analytical techniques for volatiles: A case study using intermediate (andesitic) glasses. American Mineralogist, 87, 1077-1089.

King, P.L., McMillan, P.F., and Moore, G. (2004) Infrared spectroscopy of silicate glasses with application to natural systems. In P.L. King, M.S. Ramsey, and G.A. Swayze, Eds.

Infrared Spectroscopy in Geochemistry, Exploration Geochemistry and Remote Sensing, 33, p. 93-133. Mineralogical Association of Canada, Short Course.

Larsen, J.F., and Gardner, J.E. (2004) Experimental study of water degassing from phonolite melts: Implications for volatile oversaturation during magmatic ascent. Journal of Volcanology and Geothermal Research, 134, 109-124.

Liu, Y., Zhang, Y.X., and Behrens, H. (2004) H_2O diffusion in dacitic melts. Chemical Geology, 209, 327-340.

Lowernstern, J.B. and Pitcher, B.W., submitted. Analysis of H_2O in silicate glass using attenuated total reflectance (ATR) micro-FTIR spectroscopy. American Mineralogist.

Ludwig, K.R. (2003) Isoplot 3.00: A Geochronological Toolkit for Microsoft Excel. Berkeley Geochronology Center Special Publication, 4, 71 pp. http://www.bgc.org/isoplot_etc/software.html

Lui, D.K. (2005) The Effects of Water on Basalt-Rhyolite Interactions in Volcanic Systems. M.Sc. Thesis, University of Western Ontario, London ON Canada.

Mandarino, J.A. (1976) The Gladstone-Dale relationship- Part I: Derivation of new constants. Canadian Mineralogist, 14, 498-502.

Mandeville, C., Webster, J., Rutherford, M., Taylor, B., Timbal, A., and Faure, K. (2002) Determination of molar absorptivities for infrared absorption bands of H_2O in andesitic glasses. American Mineralogist, 87, 813-821.

McMillan, P.F., and Hofmeister, A. (1988) Infrared and Raman Spectroscopy. In F.C. Hawthorne, Ed. Spectroscopic Methods in Mineralogy and Geology, 18, p. 99-159. Mineralogical Society of America, Blacksburg, VA.

Mercier, M., Di Muro, A., Giordano, D., Métrich, N., Lesne, P., Pichavant, M., Scaillet, B., Clocchiatti, R., Montagnac, G. (2009) Influence of glass polymerisation and oxidation on micro-Raman water analysis in alumino-silicate glasses. Geochimica et Cosmochimica Acta 73, 197-217.

Métrich, N., and Wallace, P.J. (2008) Volatile abundances in basaltic magmas and their degassing paths tracked by melt inclusions. In K.D. Putirka, and F.J. Tepley III, Eds. Reviews in Mineralogy and Geochemistry, 69, p. 363-402. Mineralogical Society of America, Washington DC.

Mongrain, J., Larsen, J.F., and King, P.L. (2008) Rapid H_2O exsolution, gas loss, and bubble collapse observed experimentally in K-phonolite melts. Journal Volcanology and Geothermal Research, doi: 10.1016/j.jvolgeores.2008.01.026.

Moore, G., and Carmichael, I.S.E. (1998) The hydrous phase equilibria (to 3 kbar) of an andesite and basaltic andesite from western Mexico: constraints on water content and conditions of phenocryst growth. Contributions to Mineralogy and Petrology, 130, 304-319.

Moore, G., Chizmeshya, A., and McMillan, P.F. (2000) Calibration of a reflectance FTIR method for determination of dissolved CO_2 concentration in rhyolitic glass. Geochimica et Cosmochimica Acta, 64, 3571-3579.

Newman, S., Stolper, E.M., and Epstein, S. (1986) Measurement of water in rhyolitic glasses: calibration of an infrared spectroscopic technique. American Mineralogist, 71, 1527-1541.

Nichols, A. R. L. and Wysoczanski, R. J. (2007) Using micro-FTIR spectroscopy to measure volatile contents in small and unexposed inclusions hosted in olivine crystals. Chemical Geology, 242, 371-384.

Nowak, M. and Behrens, H. (1995) The speciation of water in haplogranitic glasses and melts determined by in situ near-infrared spectroscopy. Geochimica et Cosmochimica Acta, 59, 3445-3450.

Paterson, M.S. (1982) The determination of hydroxyl by infrared absorption in quartz, silicate glasses and similar materials. Bulletin Minéralogie, 105, 20-29.

Pauly, B.D., Schiffman, P., Zierenberg, R.A., and Clague, D.A. (2011) Environmental and chemical controls on palagonitization. Geochemistry, Geophysics, Geosystems, 12, Q12017, doi: 10.1029/2011GC003639.

Perfit, M.R., Fornari, D.J., Malahoff, A., and Embley, R.W. (1983) Geochemical studies of abyssal lavas recovered by DSRV Alvin from Eastern Galapagos Rift, Inca Transform, and Ecuador Rift. 3. Trace element abundances and petrogenesis. Journal of Geophysical Research, 88, 10,551-10,572.

Perfit, M.R., Ridley, W.I., and Jonasson, I.R. (1999) Geologic, petrologic, and geochemical relationships between magmatism and massive sulfide mineralization along the Eastern Galapagos Spreading Center. In C.T. Barrie and M.D. Hannington, Eds. Volcanic-associated Massive Sulfide Deposits: Processes and Examples in Modern and Ancient Settings, Reviews in Economic Geology, 8, 75-100.

Silver, L.A. (1988) Water in Silicate Glasses. Ph.D. dissertation, Dept. Geological Planetary Sciences, p. 310. California Institute of Technology, Pasadena.

Sinton, J.M., Ford, L.L., Chappell, B., and McCulloch, M.T. (2003) Magma genesis and mantle heterogeneity in the Manus Back-arc Basin, Papua New Guinea. Joural of Petrology, 44, 159-195. doi: 10.1093/petrology/44.1.159

517 Stolper, E. (1982a) The speciation of water in silicate melts. Geochimica et Cosmochimica Acta,
518 46, 2609-2620.
519 Stolper, E. (1982b) Water in silicate glasses: An infrared spectroscopic study. Contributions to
520 Mineralogy and Petrology, 81, 1-17.
521 Thomas, R. (2000) Determination of water contents of granite melt inclusions by confocal laser
522 Raman microprobe spectroscopy. American Mineralogist, 85, 868-872.
523 Thomas, R., Kamenetsky, V.S., and Davidson, P. (2006) Laser Raman spectroscopic
524 measurements of water in unexposed glass inclusions. American Mineralogist, 91, 467-
525 470.
526 Thomas, R., Métrich, N., Scaillet, B., Kamenetsky, V.S., and Davidson, P. (2008a)
527 Determination of water in Fe-rich basalt glasses with confocal micro-Raman
528 spectroscopy. Zeitschrift für Geologische Wissenschaften, 36, 31-37.
529 Thomas, S.-M., Thomas, R., Davidson, P., Reichart, P., Koch-Müller, M., and Dollinger, G.,
530 (2008b) Application of Raman spectroscopy to quantify trace water concentrations in
531 glasses and garnets, American Mineralogist, 93, 1550-1557
532 Wallace, P., and Anderson Jr., A.T. (2000) Volatiles in magmas. In H. Siggurdsson, Ed.
533 Encyclopedia of Volcanoes, p. 149-170. Academic Press, San Diego.
534 Westrich, H.R. (1987) Determination of water in volcanic glasses by Karl-Fischer titration.
535 Chemical Geology, 63, 335-340.
536 Zajacz, Z., Halter, W., Malfait, W.J., Bachmann, O., Bodnar, R.J., Hirschmann, M.M.,
537 Mandeville, C.W., Morizet, Y., Müntener, O., Ulmer, P., and Webster, J.D. (2005) A
538 composition-independent quantitative determination of the water content in silicate

glasses and silicate melt inclusions by confocal Raman spectroscopy. Contributions to Mineralogy and Petrology 150, 631-642.

Zhang, Y., Xu, Z., and Behrens, H. (2000) Hydrous species geospeedometer in rhyolite: improved calibration and application. Geochimica Cosmochimica Acta, 64, 3347-3355.

Figure Captions

FIGURE 1: (a) Reflectance spectrum for calc-alkaline andesite, MHA-23, with insets showing the total H_2O (H_2O_{tot}), molecular CO_2 ($CO_{2\ mol}$) and CO_3^{2-} bands. Note that it is difficult to evaluate where a baseline should be drawn in the case of the C-O species bands. (b) Reflectance spectrum for calc-alkaline andesite MHA-41 showing the sigmoidal molecular H_2O (H_2O_{mol}) band at ~1620 cm^{-1}. Note that it is difficult to evaluate where a baseline should be drawn in the case of this sigmoidal band. (c) KK-Abs. spectrum for MHA-23 with insets showing H_2O_{tot}, $CO_{2\ mol}$ and CO_3^{2-} bands. (d) KK-Abs. spectrum for MHA-41 showing the H_2O_{mol} band at ~1620 cm^{-1}. The volatile contents for both of these samples are given in Table 2.

FIGURE 2: KK-Abs. band height for the ~3600 cm^{-1} band versus total H_2O (H_2O_{tot}) wt.% determined via manometry or secondary ion mass spectrometry for a range of glass compositions: basalt, calc-alkaline andesite, alkali andesite, phonolite and rhyolite.

FIGURE 3: KK-Abs. band height for the ~1620 cm^{-1} band versus molecular H_2O (H_2O_{mol}) wt.% determined via transmission IR spectroscopy for calc-alkaline andesitic glasses (King et al., 2002).

FIGURE 4: KK-Abs. band height for the ~2350 cm^{-1} band versus molecular CO_2 ($CO_{2\ mol}$) wt.% determined via transmission IR spectroscopy for calc-alkaline andesitic glasses (King et al., 2002).

FIGURE 5: KK-Abs. band height for ~1520 cm^{-1} band versus CO_3^{2-} wt.% determined via transmission IR spectroscopy for calc-alkaline andesitic glasses (King et al., 2002).

FIGURE 6: Slope of the calibration line (*m*) for total H_2O (H_2O_{tot}) concentration versus calculated refractive index, *n* for the range of compositions studied. Data are shown for both a linear

least squares regression approach (no error bars for *m*) and also a robust regression approach (with error bars for *m*). Note that a range of basaltic compositions were used in the calibration and only an average is reported.

FIGURE 7: (a) Reflectance spectrum for a wafer of representative calc-alkaline andesite glass (MHA-23) placed on a gold-coated glass slide. The numbers refer to the KK-Abs. of the band. (b) Transmission spectrum in absorbance units for a representative calc-alkaline andesite glass (MHA-23). Note that the KK-Abs. values are greater for the wafer in reflectance mode than the wafer in transmission mode.

FIGURE 8: (a) Reflectance spectra of an initially 60 μm thick calc-alkaline andesite MHA-31 wafer that has been polished or roughened on its back to 1 μm, 40 μm and 90 μm. (b) Reflectance spectra of an initially 63 μm thick calc-alkaline andesite MHA-44 wafer that has been polished to 1 μm or roughened to 130 μm on its back and set in epoxy. Note that with increased roughening the intensity decreases in the downward pointing transmission bands (T) related to C-O-H species and the intensity increases in the reflectance band (R) at ~1000 cm^{-1} related to O-Si-O asymmetric stretching.

FIGURE 9: KK-Abs. spectra for two samples of calc-alkaline andesite MHA-44 wafer: (i) solid spectrum is from a wafer (initially 63 μm thick) roughened to 130 μm on its back and set in epoxy; and (ii) dashed spectrum is from a thick glass that was singly polished.

FIGURE 10: (a) KK-Abs. band height for the ~3600 cm^{-1} band versus total H_2O (H_2O_{tot}).wt.% in calc-alkaline andesites measured using either a MCT-A or MCT-A* detector. (b) KK-Abs. band height for the ~3600 cm^{-1} band versus total H_2O (H_2O_{tot}).wt.% in phonolites measured in King's lab and Larsen's lab.

590

591 **Table 1: Compositions of glasses used for calibrations in King's lab.**

592

	Basalt	Calc-alk. andesite	Alkaline andesite	Phonolite	Rhyolite
wt.%, normalized to 100%					
SiO_2	53.69 (2.69)	60.62	63.68	57.31	75.58 (1.52)
TiO_2	1.17 (0.95)	0.89	0.64	0.24	0.17 (0.13)
Al_2O_3	14.29 (2.17)	18.57	17.60	23.12	13.57 (0.83)
FeO	10.71 (2.77)	5.56	3.89	1.63	1.31 (0.39)
MgO	6.51 (3.00)	2.71	2.70	0.10	0.18 (0.12)
CaO	10.82 (2.18)	6.05	5.74	0.66	0.88 (0.43)
Na_2O	2.25 (0.58)	4.67	4.12	11.22	4.36 (0.09)
K_2O	0.56 (0.47)	0.92	1.64	5.72	3.93 (0.30)
Reference*	1	2	3	4	5

593

594 *1. Galapagos basalt # 1652-5 (Perfit et al., 1983, 1999), Manus Basin basalts #15-4, 2249 and
595 18-3 (Sinton et al., 2003) and experimental basalt DL414 (Lui, 2005). 2. Mount Hood andesite
596 (King et al., 2002). 3. Mascota andesite (Moore and Carmichael, 1998). 4. Laacher See Tephra
597 phonolite (Larsen and Gardner, 2004). 5. PCD and M3M rhyolites (Westrich, 1987).

598 **Table 2: Results of KK-Abs. measurements on calc-alkaline andesite glasses in King's lab.**

Sample	Method for H_2O_{tot}	Volatile concentrations (wt.%)				KK-Abs.values (± 10% rel.unless noted)				
		H_2O_{tot} ±10%rel.	H_2O_{mol}	$CO_{2\ mol}$	CO_3^{2-}	3600 cm^{-1} (H_2O_{tot})	1620 cm^{-1} (H_2O_{mol})	2350 cm^{-1} (CO_{2mol})	1520 cm^{-1} (CO_3^{2-})	3600 cm^{-1} (H_2O_{tot}) with MCT-A*
MHA23	SIMS	0.76	nd	0.077 (0.002)	0.337 (0.005)					
23-1						0.0035		0.0019	0.00074	
23-2						0.0046		0.0024	0.00100	
23-3						0.0041		0.0019	0.00076	
23y						0.0031		na		
MHA26	SIMS	2.43	0.75 (0.07)	0.033 (0.002)	0.373 (0.028)					
26-1						0.013	0.00130	0.0012	0.0005	0.0084 (0.0002)
26-2						0.014	0.00137	0.0013	0.0006	
26-3						0.013	0.00150	0.0011	0.0007	
26y						0.013	0.00160			
MHA27	SIMS	0.85	nd	0.077 (0.001)	0.283 (0.016)					
27-1						0.0038		0.00200	0.0007	0.0012
27-2						0.0032		0.00187	0.0008	0.0013 (0.0003)
27-3						0.0043		0.00204	0.0004	
MHA30	Man.	2.48	1.09 (0.09)	0.004	0.076 (0.011)					
30-1						0.0140	0.00213	nd	0.0004	
30-2						0.0134	0.00180	nd	0.0002	
30-3						0.0144	0.00218	nd		
MHA31	Man.	1.09	0.36 (0.03)	0.009 (0.001	0.061 (0.032)					
31-1						0.0076	0.00047	nd	0.0001	
31-2						0.0079	0.00050	0.00024	0.0002	
31-3						0.0073	0.00044	0.00044	0.0001	
MHA41	Man.	2.69	1.34 (0.06)	0.014 (0.002)	0.323 (0.048)					
41-1	Man.					0.019	0.00271		0.0004	
41-2	Man.					0.020	0.00327		0.0005	
41-3						0.020	0.00300			
MHA44	Man.	3.34	2.02 (0.19)	0.014 (0.002)	0.483 (0.040)					
44-1	Man.					0.0240	0.0051		0.0012	0.0188 (0.0006)
44-2	Man.					0.0230	0.0047	0.00037	0.0013	0.0156 (0.0002)
44-3						0.0245	0.0051	0.00034	0.0012	0.0175 (0.0003)
J12	SIMS	3.39	2.20 (0.28)	0.009 (0.001)	0.575 (0.054)					
J12-1	SIMS					0.0251		na	0.0012	0.0165 (0.0017)
J12-2	SIMS									0.0169 (0.0017)
J12-3										0.0175 (0.0018)

599 **Table 3: Results of KK-Abs. measurements on four glass compositions.**

				KK-Abs.values (± 10% rel. unless noted)	
Sample	**Analysis #**	**H_2O_{tot} method**	**H_2O_{tot} wt.% (± 10% rel. unless noted)**	**King's lab 3600 cm^{-1} (H_2O_{tot})**	**Larsen's lab 3600 cm^{-1} (H_2O_{tot})**
Alkali andesites					
MA512	MA512-1	Manometry	0 (0.01)	0	
	MA512-2	Manometry	0 (0.01)	0	
M12-1	M12-1-1	Manometry	2.62 (0.01)	0.0163	
	M12-1-2	Manometry	2.62 (0.01)	0.0161	
	M12-1-3	Manometry	2.62 (0.01)	0.0173	
M12-2	M12-2-2	Manometry	5.03 (0.01)	0.0298	
	M12-2-3	Manometry	5.03 (0.01)	0.0312	
	M12-2-4	Manometry	5.03 (0.01)	0.0323	
M12-4	M12-4-1	Manometry	6.76 (0.01)	0.0450	
	M12-4-2	Manometry	6.76 (0.01)	0.0453	
Basalts					
ManB_2249	Man2249-1	Trans IR	1.19	0.0103	
	Man2249-2	Trans IR	1.19	0.0101	
ManB15-4	Man15-4-1	Trans IR	1.32	0.0134	
	Man15-4-2	Trans IR	1.32	0.0129	
Gal1652	Gal1652-5a	Trans IR	1.38	0.0123	
ManB-18-3	Man18-3-1	Trans IR	1.44	0.0127	
	Man18-3-2	Trans IR	1.44	0.0126	
	Man18-11-1	Trans IR	1.49	0.0154	
	Man18-11-2	Trans IR	1.49	0.0119	
DL0414	DL0414_r1	Trans IR	4.63	0.0368	
	DL0414_r2	Trans IR	4.63	0.0357	
	DL0414_r4	Trans IR	4.63	0.0354	
Phonolites					
LPG1	LPG1	Trans IR	4.68 (0.50)	0.0273	
	LPG1-2	Trans IR	4.68 (0.50)	0.0262	
	LPG1-3	Trans IR	4.68 (0.50)	0.0267	
LPG1a	LPG1a_1	Trans IR	4.13 (0.23)	0.0222	
	LPG1a_2	Trans IR	4.13 (0.23)	0.0223	
	LPG1a_3	Trans IR	4.13 (0.23)	0.0205	
	LPG1a_4	Trans IR	4.13 (0.23)	0.023	
LPG3	LPG3-1	Trans IR	4.55 (0.08)		
	LPG3-1	Trans IR	4.55 (0.08)		
	LPG3-2	Trans IR	4.55 (0.08)		
	LPG3-3	Trans IR	4.55 (0.08)		
LHAE2	LHAE2-1	Trans IR	2.93 (0.15)	0.0181 (0.0007)	
	LHAE2-2	Trans IR	2.93 (0.15)		
	LHAE2-3	Trans IR	2.93 (0.15)	0.0176 (0.0009)	
	LHAE2-4	Trans IR	2.93 (0.15)	0.0170 (0.0013)	
LHAE3	LHAE3-1	Trans IR	4.99 (0.72)	0.0279 (0.0001)	0.0330
	LHAE3-2	Trans IR	4.99 (0.72)	0.0276 (0.0002)	
	LHAE3-3	Trans IR	4.99 (0.72)	0.0282 (0.0003)	
LHAE4	LHAE4-1	Trans IR	4.25 (0.25)	0.0248 (0.0005)	0.0268
	LHAE4-2	Trans IR	4.25 (0.25)	0.0250 (0.0001)	
	LHAE4-3	Trans IR	4.25 (0.25)	0.0249 (0.0003)	
LHAE5	LHAE5-1	Trans IR		0.0290 (0.0003)	0.0312
	LHAE5-2	Trans IR		0.0287 (0.0001)	0.0329
	LHAE5-3	Trans IR		0.0282 (0.0001)	
LPG4	LPG4-1	Trans IR	3.77 (0.05)	0.0260 (0.0001)	0.0302
	LPG4-2	Trans IR	3.77 (0.05)	0.0277 (0.0004)	
	LPG4-3	Trans IR	3.77 (0.05)	0.0275 (0.0001)	
LPG6	LPG6-1	Trans IR	3.39 (0.10)	0.0177 (0.0005)	0.0251
	LPG6-2	Trans IR	3.39 (0.10)	0.0168 (0.0007)	0.0270
	LPG6-3	Trans IR	3.39 (0.10)	0.0194 (0.0006)	0.0266
	LPG6-4	Trans IR	3.39 (0.10)	0.0199 (0.0004)	
LSN1	LSN1-1	Trans IR		0.0294 (0.0005)	0.0430
	LSN1-2	Trans IR		0.0302 (0.0001)	0.0396
	LSN1-3	Trans IR		0.0299 (0.0006)	

600 **Table 3 (ctd.)**

Sample	Analysis #	H_2O_{tot} method	H_2O_{tot} wt.%	KK-Abs.values (± 10% rel. unless noted) King's lab 3600 cm^{-1} (H_2O_{tot})	KK-Abs.values (± 10% rel. unless noted) Larsen's lab 3600 cm^{-1} (H_2O_{tot})
Phonolites (ctd.)					
LST3-40-1	LST3-40-1-1	Trans IR	0 (0.10)	0.0035 (0.0004)	0.0045
	LST3-40-1-2	Trans IR	0 (0.10)	0.0030 (0.0001)	
	LST3-40-1-3	Trans IR	0 (0.10)	0.0030 (0.0002)	
Rhyolites					
UTR2	UTR2	Manometry	0.09 (0.04)	0.0012	
PCD	PCDA	Manometry	0.13 (0.04)	0.0013	
	PCDB	Manometry	0.17 (0.04)	0.0015	
2N	2N	Manometry	2.07 (0.29)	0.0097	
	2N_2	Manometry	2.07 (0.29)	0.0103	
	2N_3	Manometry	2.07 (0.29)	0.0089	
M3N	M3N	Manometry	2.94 (0.16)	0.0142	
	M3N_3	Manometry	2.94 (0.16)	0.0145	
	M3N_4	Manometry	2.94 (0.16)	0.0141	
M6N	M6N	Manometry	5.11 (0.38)	0.0239	
	M6N_3	Manometry	5.11 (0.38)	0.0257	
	M6N_4	Manometry	5.11 (0.38)	0.0259	

601

602

Table 4: Molar Si+Al, calculated refractive indices, fit parameters and root mean square error of prediction for H_2O_{tot} calibrations for five different glass compositions measured in King's lab.

	Basalt	Calc-alk. andesite	Alkaline andesite	Phonolite	Rhyolite
Molar Si+Al	0.66 (0.04)	0.76	0.78	0.73	0.85 (0.00)
Refr. index	1.590 (0.013)	1.544	1.533	1.506	1.491 (0.005)
Least squares fit results for H_2O_{tot}					
Slope	0.0080	0.0065	0.0064	0.0058	0.0049
m	125	154	156	172	204
RMSEP	0.12	0.14	0.20	0.19	0.10
Robust regression fit results for H_2O_{tot}					
Slope	0.00795 (+0.00080 –0.00071)	0.00697 (+0.00034 –0.00150)	0.00627 (+0.00044 –0.00034)	0.00522 (+0.00043 –0.00033)	0.00480 (+0.00018 –0.00024)
m	126 (+12/–12)	143 (+39/–7)	159 (+9/–10)	192 (+13/–15)	208 (+11/–8)
RMSEP	0.18	0.18	0.23	0.38	0.13

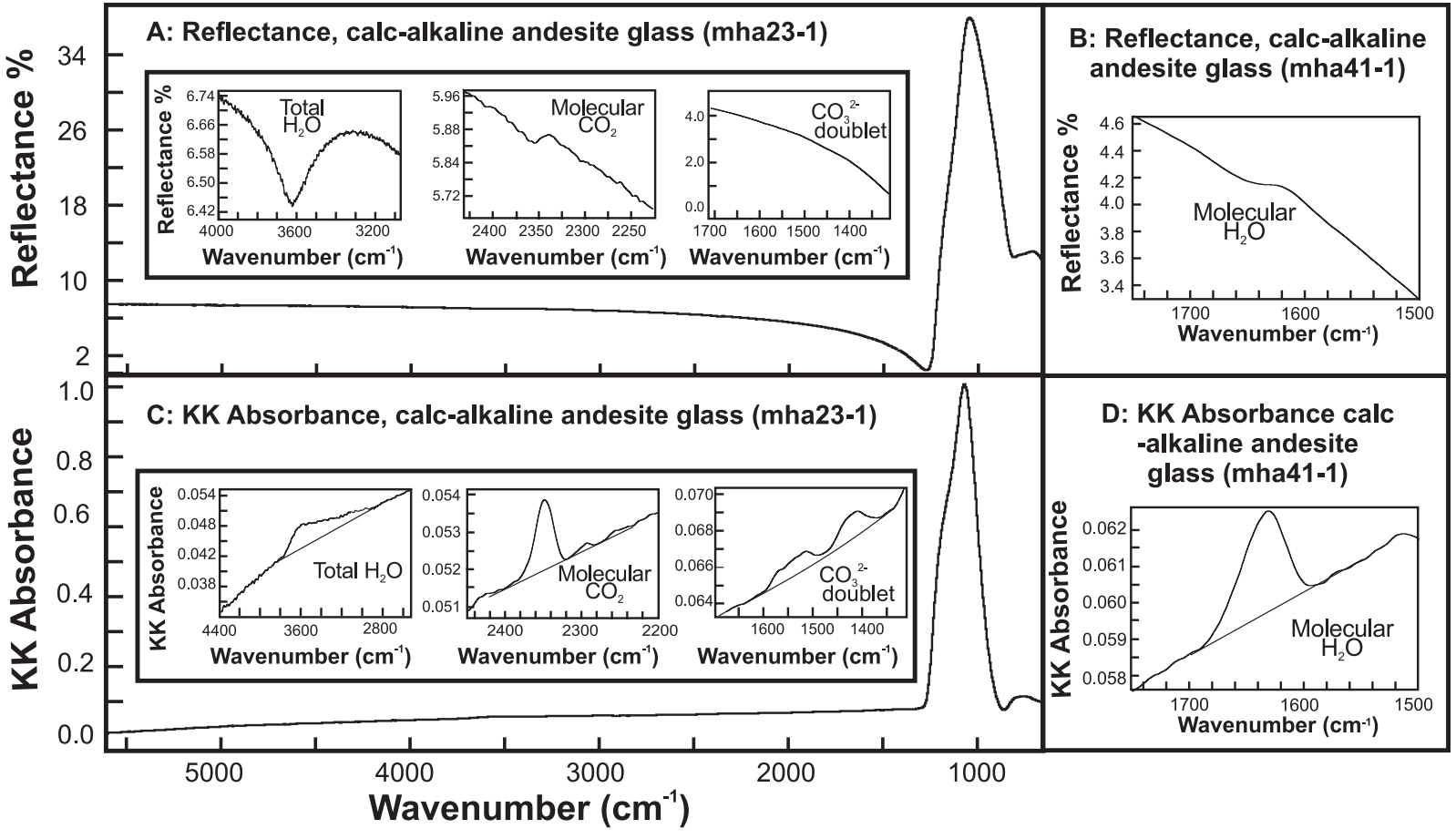

King & Larsen - FIGURE 1

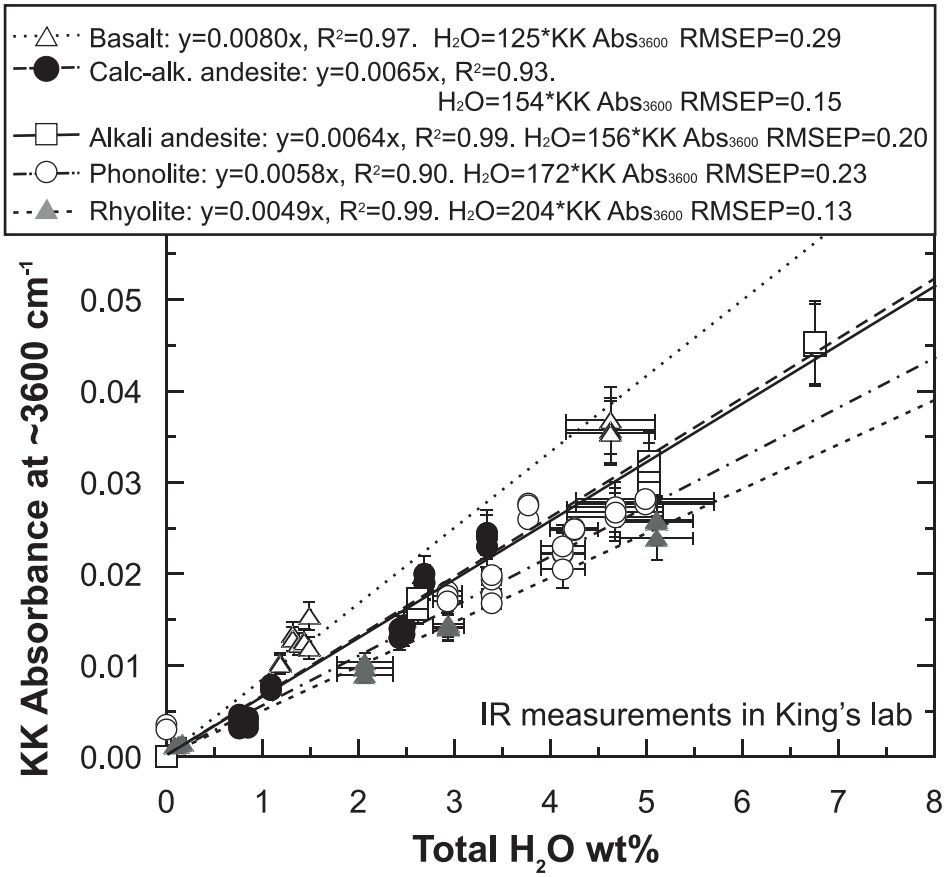

King & Larsen - FIGURE 2

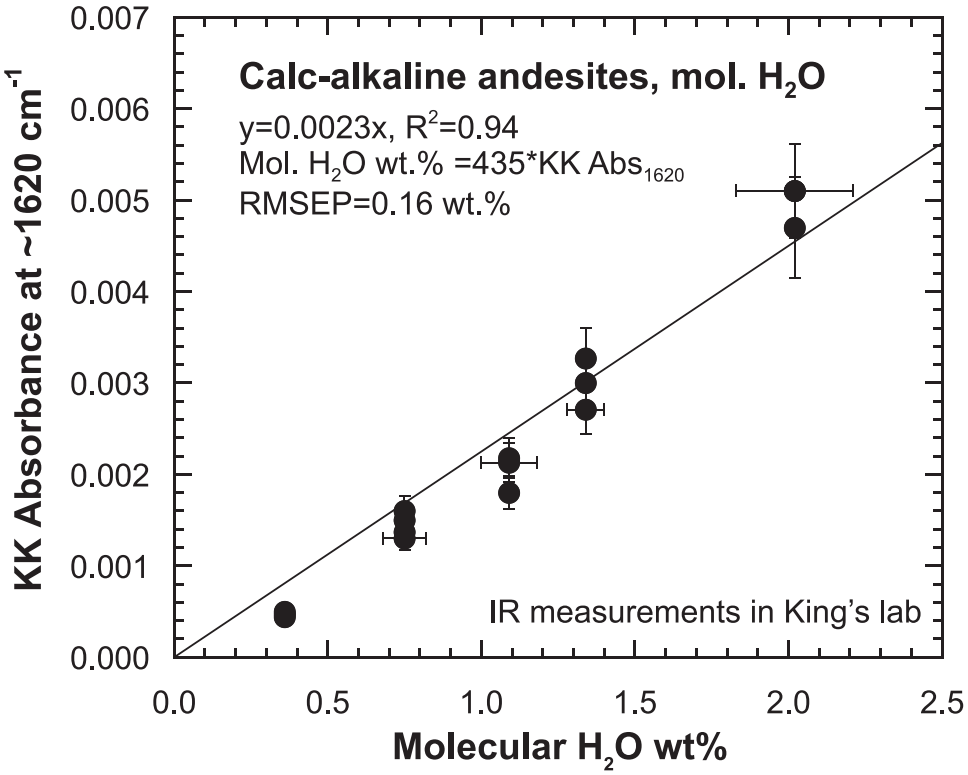

King & Larsen - FIGURE 3

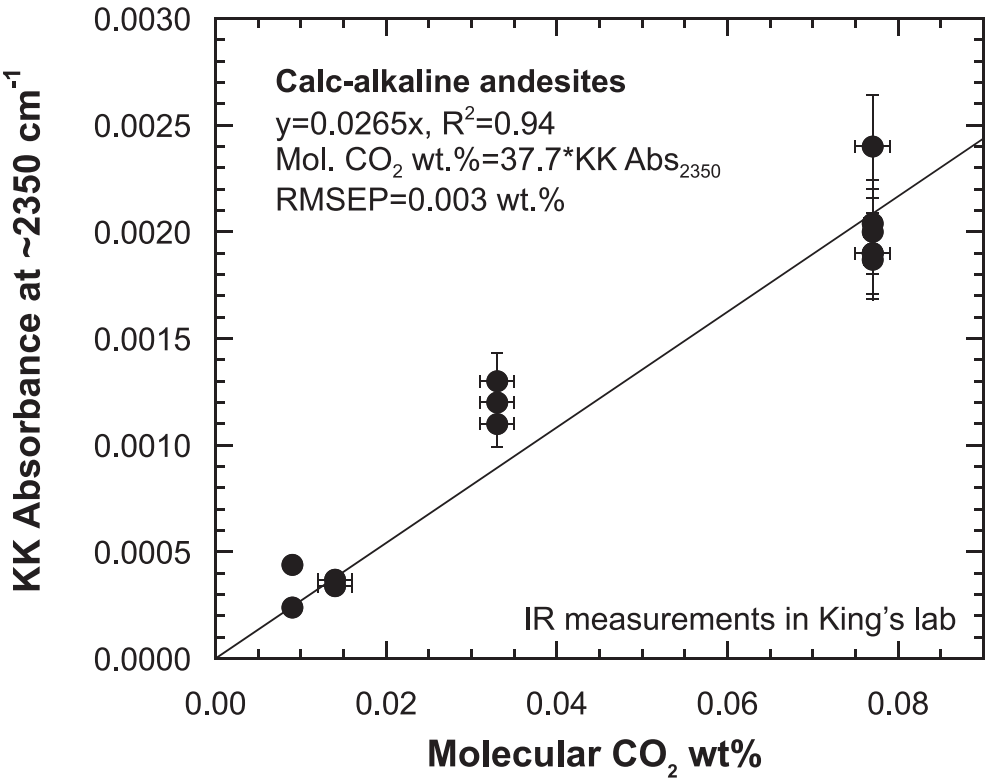

King & Larsen - FIGURE 4

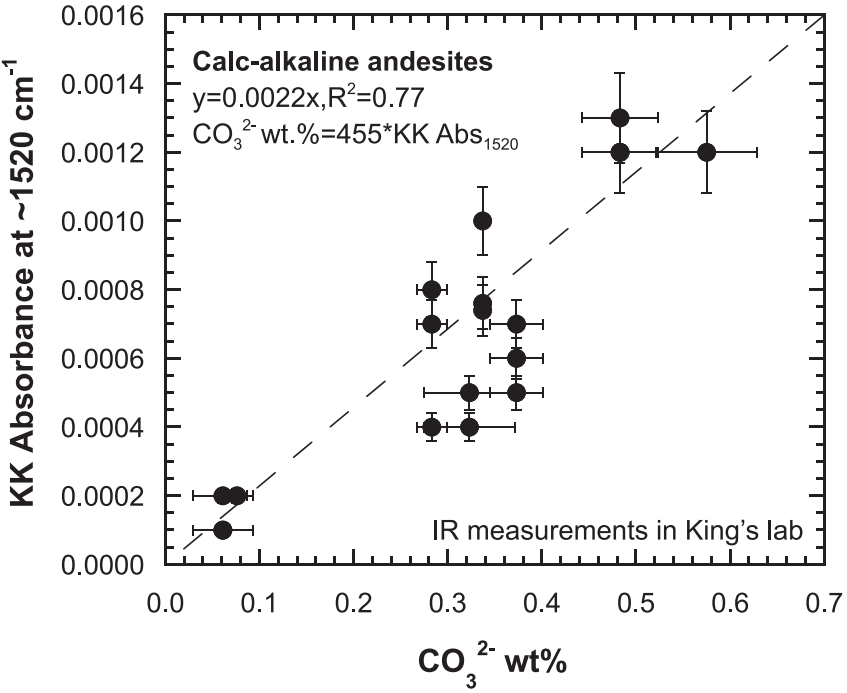

King & Larsen - FIGURE 5

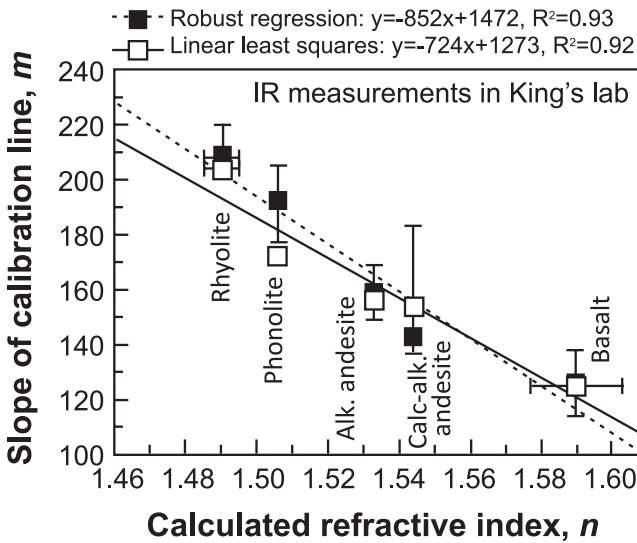

King & Larsen - FIGURE 6

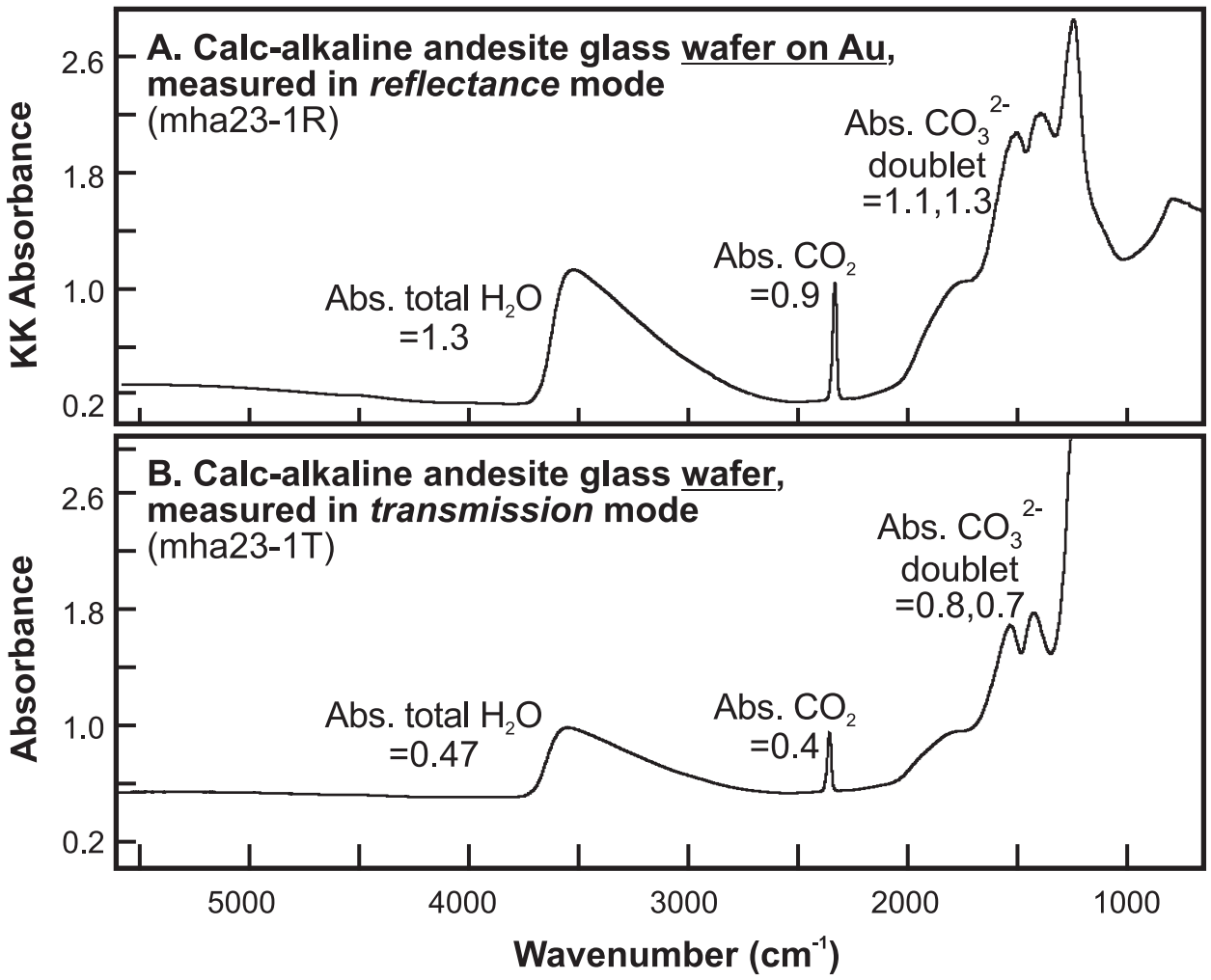

King & Larsen - FIGURE 7

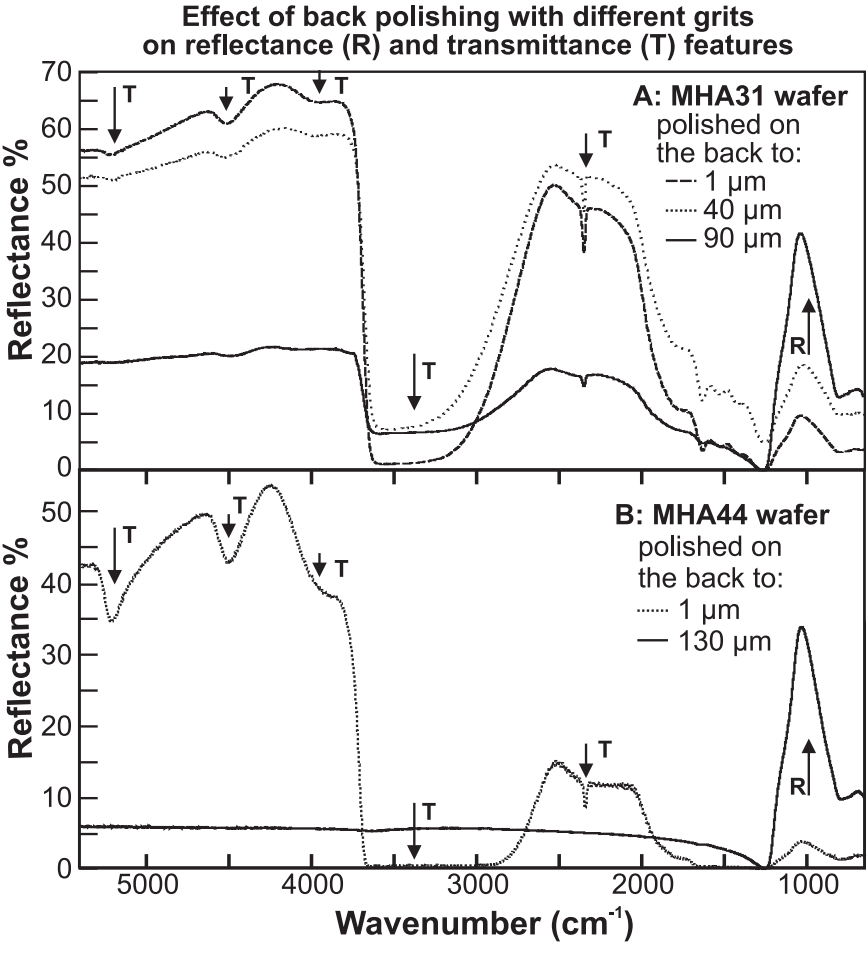

King & Larsen - FIGURE 8

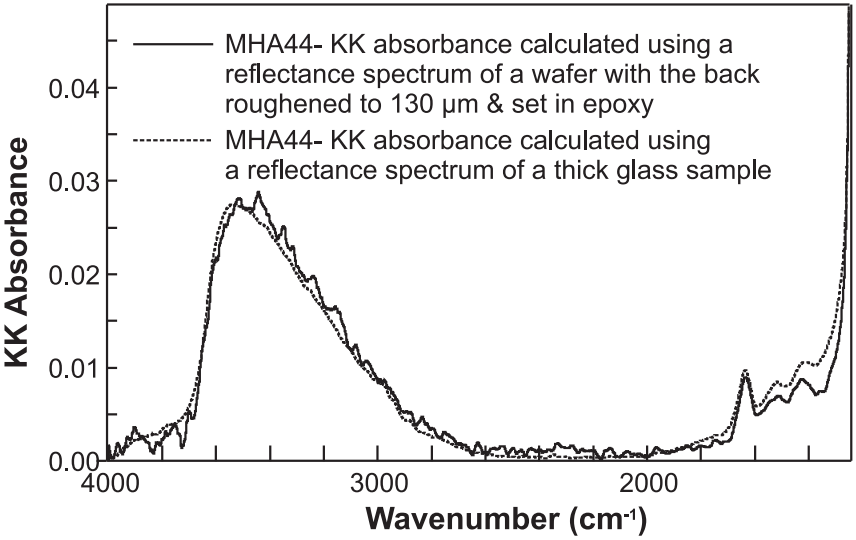

King & Larsen - FIGURE 9

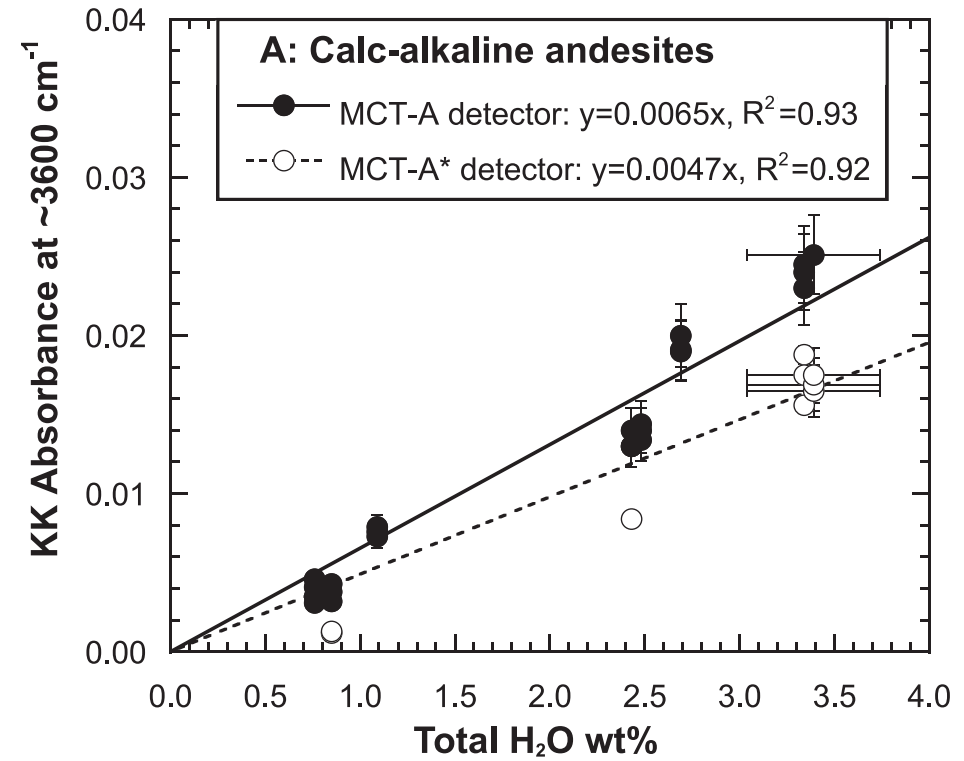

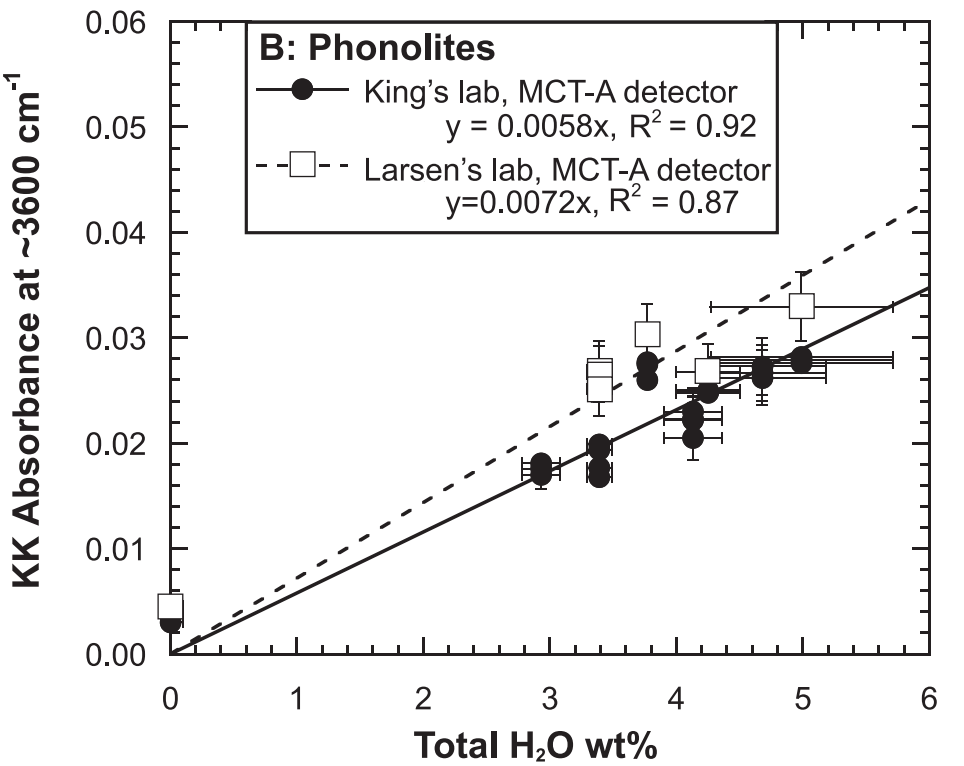

King & Larsen - FIGURE 10